Twin-pair rete ridge analysis: a computer-aided method for facilitating objective histopathological distinction between epithelial dysplasia and carcinoma in-situ of the oral mucosa

Mustafa M. Sami[1], Masahisa Saito[1, 2], Shogo Muramatsu[1], Toshihiko Mikami[3], Kamal Al-Eryani[3, 4], Faleh A. Sawair[5], Rasha Abu Eid[5], Jun Cheng[3], Hisakazu Kikuchi[1], Takashi Saku[3]

[1]Department of Electrical and Electronics Engineering, Graduate School of Science and Technology, Niigata University, Niigata, Japan
[2]Imaging Science and Engineering Laboratory, Tokyo Institute of Technology, Yokohama, Japan
[3]Division of Oral Pathology, Niigata University Graduate School of Medical and Dental Sciences, Niigata, Japan
[4]Department of Oral Medicine and Pathology, Faculty of Dentistry, Sana'a University, Sana'a, Yemen
[5]Department of Oral and Maxillofacial Surgery, Oral Medicine, Oral Pathology and Periodontology, Faculty of Dentistry, University of Jordan, Amman, Jordan

Abstract: **Epithelial dysplasia and carcinoma in-situ (CIS) of the oral mucosa are two different borderline grades similar to each other, and it is difficult for pathologists to distinguish these two lesions on hematoxylin and eosin-stained sections only. To support objective differential diagnoses, we have developed a new computer-aided analysis system. The method was based on a comparison of the elevation levels in the drop shape between twin-pairs of neighboring rete ridges. The dissimilarity of the drop shape was defined by the roundness difference between a pair of rete ridge units. All the steps were performed using a graphical user interface. The similarity levels in epithelial dysplasia were higher than those in CIS, whose histopathological diagnoses were conventionally made by experienced pathologists. The developed image processing method showed good promise for the computer-aided pathological assessment of oral borderline malignancies in clinical practice.**

[*Oral Med Pathol* 2010; 14: 89-97 doi: 10.3353/omp.14.89]

Key words: **borderline malignancies, image analysis, oral mucosa, rete ridges, twin pairs**

Correspondence: Hisakazu Kikuchi, Department of Electrical and Electronics Engineering, Niigata University Graduate School of Science and Technology, 2-8050 Ikarashi, Nishi-ku, Niigata 950-2181, Japan
Phone: +81-25-262-7791, Fax: +81-25-262-6932, E-mail: kikuchi@eng.niigata-u.ac.jp

Introduction

Oral cancer is one of the six most common human cancers in the world (1). While cigarette smoking and alcohol drinking are major risk factors in Western countries, the habits of chewing betel quid, tobacco, or qat leaves are major risk factors in the causation of oral cancer in many Asian and Arabic cultures (2-3). In Yemen and India, oral cancers are the most common types of cancer, representing up to 30% of all body cancers (2, 4). Oral squamous cell carcinoma (SCC) accounts for more than 90% of all oral cancers. Oral SCCs have been thought to develop from pre-malignant lesions (5), such as leukoplakia, which histopathologically includes two major classes of borderline malignancies: epithelial dysplasia and CIS.

As it is not always easy for pathologists to make an accurate diagnosis of these borderline malignancies by using only hematoxylin-eosin stained specimens (6), the development and use of computer tools for analyzing microscopic images of oral tissues could aid in objective analysis (7). Oral epithelial dysplasia and CIS are two different grades which should be distinguished from each other because CIS develops into invasive SCC. However, how to differentiate between them due to histological similarities is not always clear to pathologists (8-9), and diagnoses based on subjectivities or the personal experiences may differ from hospital to hospital, and accordingly, pathologists may feel uncertain when making such diagnostic decisions based on but a few commonly-accepted standards. Therefore, accurate histopathological grading methods are needed to commence category-specific treatments.

At the histopathological level, the shape of the rete ridges is a histological key feature and is considered to be highly important by pathologists when grading oral borderline malignancies (6, 10). The rete ridge contour can be defined as the edge segment that separates the epithelial zone from the connective tissue. The contour of the rete ridges is fixed by a basement membrane, which is a sheet-

like extracellular matrix interface between the epithelial zone and the underlying connective tissue. In contrast to normal rete ridges, those in the process of malignant transformation become enlarged in the direction of underlying connective tissues. Their most characteristic form at this stage is a "drop shape" as indicated in the WHO classification (10), and it is frequently associated with epithelial dysplasia with the characteristic two-phase appearance (11).

In this article, our aim is to introduce a new method that enables the distinction of CIS from dysplastic epithelia based on the analysis of drop shape variations of rete ridge units, providing an objective tool with promising potential for clinical use.

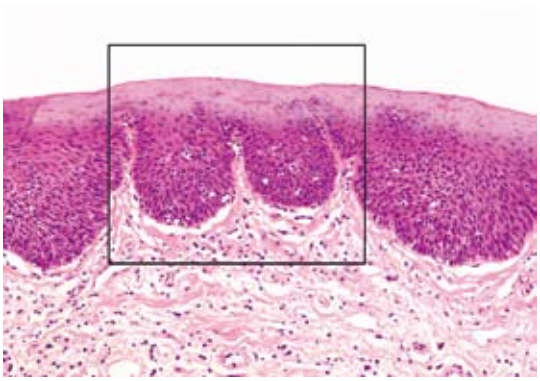

Fig. 1. Twin-pair of rete ridges in a histopathological image of oral carcinoma in-situ stained with hematoxylin and eosin (HE). The term *twin-pair* was applied for a spatially neighboring pair of rete ridges with similar shapes. Selection of twin-pairs was performed subjectively by technologists and not by pathologists.

Materials and methods

Our approach for analyzing rete ridges was divided into several well-defined stages. After image acquisition using a high resolution digital camera, we manually selected well matching twin-pairs of neighboring rete ridges from the rete ridges present in the same section. A sequence of image processing operations was applied in order to extract the contour of rete ridges. At first, saturation-based color segmentation in a hue, saturation, and value color space (HSV) was applied for the purpose of separating the epithelial zone from the rest of the tissue image. After epithelium segmentation, the main pixels at the boundary of the objects were defined and referred to as edgels. Next, a morphological operation based on dilation was applied followed by a thinning operation to connect those edgel pixels. A chain code was designed to trace the contour that represented the rete ridges. Finally, every rete ridge unit was determined and quantified for aiding differentiation of the borderline malignancies.

Histopathological preparation

All biopsy samples from the oral mucosa were fixed in formalin and processed for paraffin embedding using the standard pathological procedure. Serial paraffin sections were cut to a thickness of 5 μm with a microtome. These sections were stained with hematoxylin and eosin (HE). Thirty-three histological images from normal and dysplastic epithelia and CIS were captured by the authors who are pathologists, using a Nikon high-resolution digital camera (DXM1200C, Nikon Corporation, Tokyo, Japan) connected to a Nikon optical microscope (S-800). Images were acquired with a 10 × or 20 × objective lens at 2058 × 1536-pixel resolution on the camera. The intensity level was adjusted so the digitized images were visually acceptable to the pathologists. The rotation of the captured images was set in such a way that the upper surface of the epithelium was in a horizontal position.

Twin rete ridge selection

Twin-pairs of the rete ridge were defined as two neighboring rete ridges which resembled each other from the view point of the authors who were technologists and who had no histopathological backgrounds. Using the developed graphical user interface (GUI), which will be described later, they selected regions of interest at a glance where twin-pairs were located by specifying a cropped rectangle that fit the twin-pair area in an image as shown in Fig. 1. The rest of the distinction process was then applied to the region of interest automatically.

Image processing

Image processing operations for the automatic extraction and representation of the rete ridges (12) were performed according to a standard method described elsewhere (13). In addition, the method was simplified in order to focus on the present series of images. The rete ridge, a targeted edge segment, was obtained from the boundary pixels of the epithelial zone. The epithelium segmentation was obtained on the basis of observation of the saturation of the epithelial zone being lower than that of the lamina propria connective tissue. Thus, the captured histological images were transformed into those of the hue, saturation, and value (HSV) color space. This generated a saturation component image in which the epithelium and connective tissue zones were clearly distinguished with different contrasts over the image. The contrast of the saturation image was improved by applying an intensity adjustment operation.

A global thresholding method (13) based on Otsu's method (14) was used to determine the threshold value for segmentation. This created a bilevel image in which pixels with lower intensity values were determined as foreground pixels (ones), while all other pixels were determined as background pixels (zeros). This resulted in a bilevel image of the epithelium as a single large object. In contrast, other smaller separate objects appeared in the connective tissue. These smaller objects were located very close to the epithelium and were considered as a part of the epithelium. This was achieved by applying morphological thickening and bridging operations followed by an opening operation. The epithelial zone was determined by the largest object in the image, while the other remaining objects which were located far away from the epithelium were removed from the image. Finally, a closing operation was applied to the

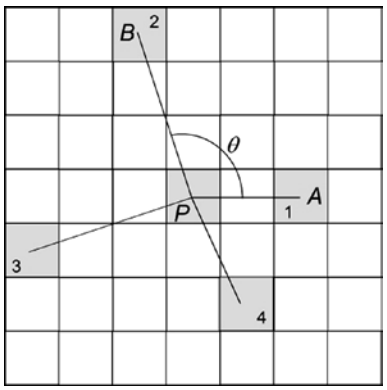

Fig. 2. Schematic concept of wide-angle edgel method. *P*, target pixel; *A*-*E*, neighboring significant pixels inside a line-of-sight distance; θ, angle between two pixels *A* and *B* around *P*. Field of view and line-of-sight distance were defined by θ and a square window centered on *P*, respectively. With respect to *P*, if the inner product between two vectors of *PA* and *PB* is not positive, *P* is an edgel which belongs to the border of the object.

segmented epithelium image.

After the epithelium segmentation, the rete ridges were extracted. They were then obtained from the main boundary pixels of the segmented epithelia. To this end, we utilized a texture-based method known as the wide-angle edgel method for selection of the edgels (15). An edgel is an edge pixel located at the boundary of an object. Its concept is explained as follows: when pixel *P* shown in Fig. 2 is assumed to be located at the boundary of an object, in which the boundary is disconnected and fragmented because of insufficient contrast and imperfect segmentation, a pair of significant pixels, for instance, *A* and *B*, defines a *field of view* (theta) within a *line-of-sight distance*. The line-of-sight distance is defined by a window of a 7 × 7-pixel size. If there are no pixels within the field of view inside the window, and if the angle *APB* is equal to or larger than 90 degrees, *P* is identified as an edgel.

Since the set of edgels obtained from the wide-angle edgel method were still disconnected, a morphological operation of dilation followed by a skeletonization thinning operation was applied to obtain a connected boundary (16-17). The generated images contained some undesirable spurious arcs which were removed by a spur removal operation. Finally, a chain coding was developed to trace the boundary of the rete ridges.

Isolation of rete ridge units

Each rete ridge unit was terminated by finding the upper peak points of the dermal papilla in the rete ridge. A half circle arc was then attached onto every pair of end-points of the rete ridge units in order to obtain a closed loop shape, and hence all rete ridge units were isolated separately. Finally, the obtained closed loop units were smoothed by assuming a 2% value of the contour descriptors (18). As a result, smoother shapes of rete ridge units were obtained, and they were resistant against insignificant variations in shape.

Numerical quantification

The aim of the presented method was to measure the drop-shape development in order to compare the malignancy levels with respect to any given twin-pair rete ridge. The roundness measurement was the shape-factor (18-19) used to quantify the drop-shape malignancy level of the rete ridge

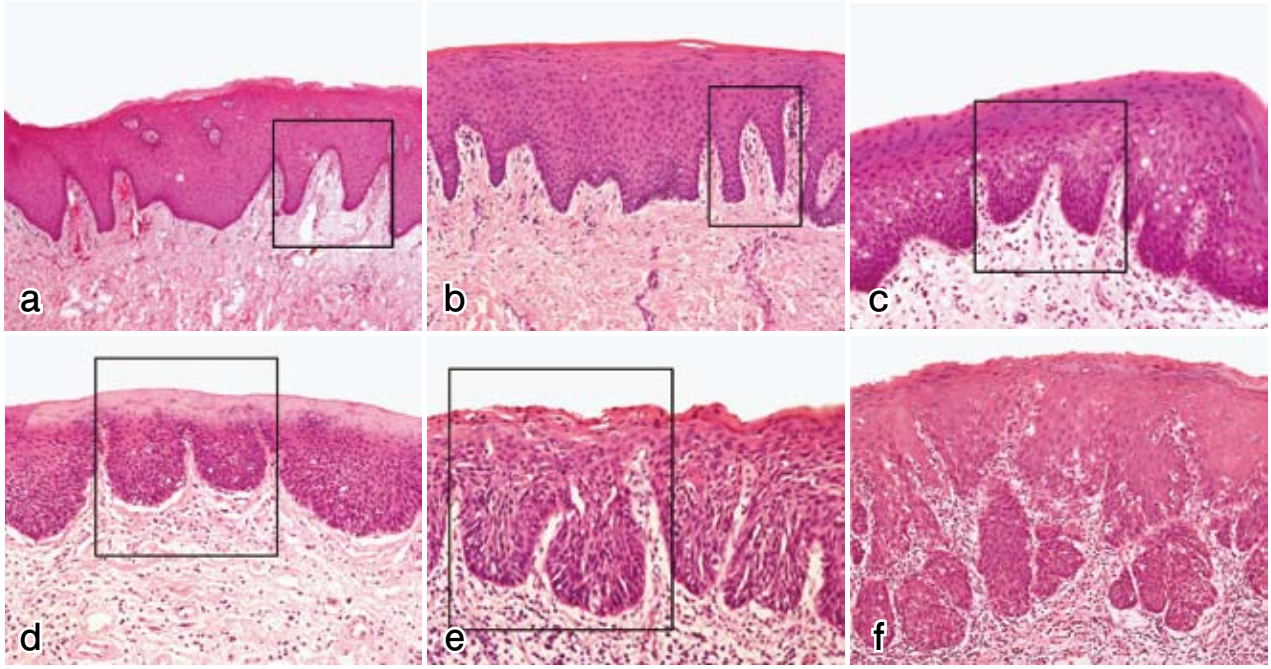

Fig. 3. Histological varieties of rete ridges among oral epithelial lesions. (**a**) Normal epithelium; (**b**) epithelial hyperplasia, (**c**) epithelial dysplasia, moderate; (**d**) carcinoma in-situ; (**e**) carcinoma in-situ with micro-invasion; (**f**) invasive squamous cell carcinoma. Rete ridge shapes definitely showed variation from normal to carcinomatous epithelia. There was an obvious tendency for their shapes to become more complicated as their levels of malignancy were elevated, although it was difficult to identify the levels for each category.

units. The roundness of a rete ridge unit was defined as

$$Roundness = \frac{area}{\pi \times \left(\frac{max\ diameter}{2}\right)^2}$$

Its maximum value was 1 in the case of a true circle and 0.5 for a half circle. The roundness was scale-invariant and rotation-invariant.

Development of graphical user interface for twin-pair analysis

For use by the pathologists of the above-mentioned analysis on digital captured histological images of oral mucosal lesions, we developed a user-friendly graphical user interface (GUI) which allowed for easy handling and analysis of histological images automatically. The software was developed using MATLAB programming language and could be run on Microsoft Windows and Macintosh operating systems.

Results

Twin rete ridges extraction

Fig. 3 shows the representative rete ridge variations selected from oral mucosal lesion samples whose diagnoses were well agreed upon by three different pathologists. As shown in Fig. 3a, normal rete ridges were random-shaped, and they projected down into slightly different directions. In epithelial dysplasia (Figs. 3b & 3c), rete ridge units of a twin-pair resembled each other, but they were delicately different from each other compared to normal ones. Rete ridges of epithelial dysplasia (Fig. 3c) and CIS (Figs. 3d & 3e) were not always clearly distinguished from each other on HE-stained sections. In invasive SCCs (Fig. 3f), their tumor cell nests were obviously different from any other lesion types mentioned above. Therefore, it was difficult to discriminate CIS from epithelial dysplasia as far as only their similar rete ridge shapes were concerned.

To obtain an objective metric for the degree of malignant transformation, we selected two neighboring rete ridges as a unit and identified them as twins, as shown in the box in Fig. 1. It was assumed based on our hypothesis that the twin-pair rete ridges should have had a more similar appearance in

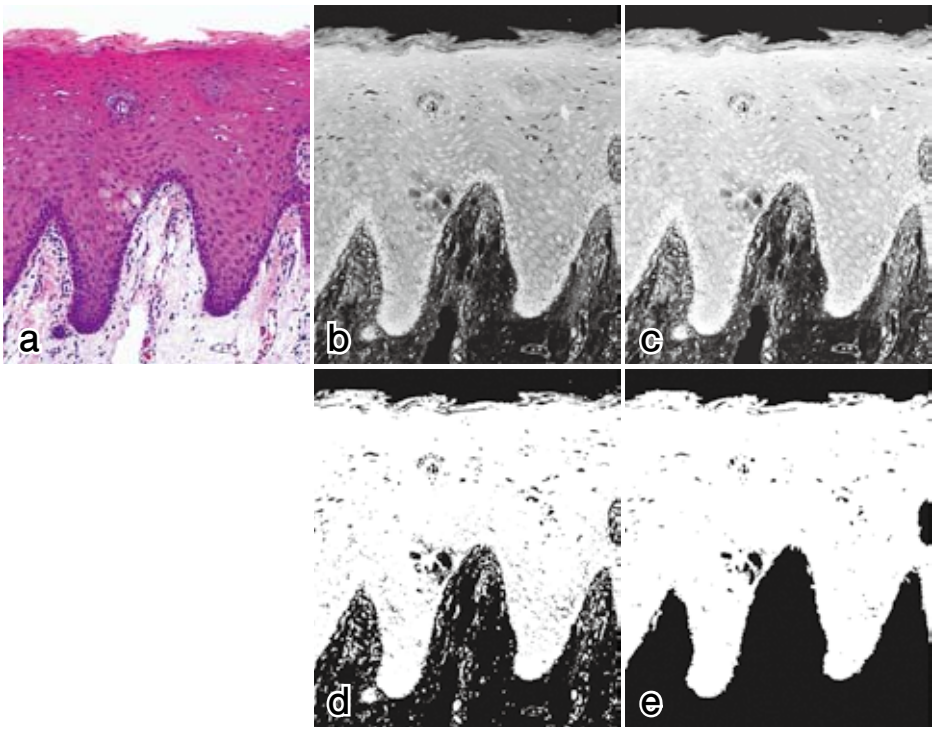

Fig. 4. Step-wise procedures of epithelium segmentation. (**a**) HE-stained image of twin-pair rete ridges captured from a normal epithelium sample; (**b**) saturation component of (a); (**c**) contrast-adjusted saturation component; (**d**) morphological operation-processed image; (**e**) final image of segmented epithelium. After intensity levels were adjusted over the image (a-c), thresholding based on Otsu's method was applied to the contours of twin-pairs (d), and they were supplemented with neighboring small objects by a thickening operation to identify the epithelial zone (e).

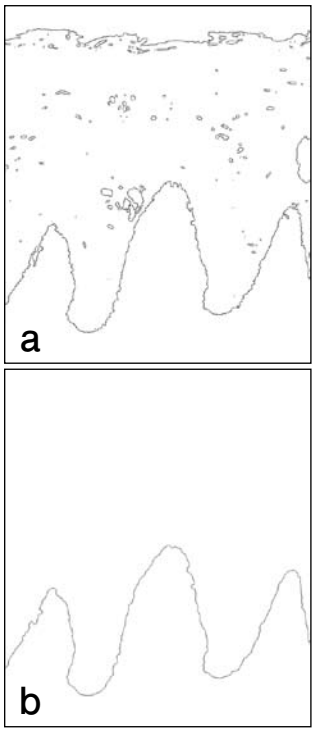

Fig. 5. Rete ridge contour extraction. (**a**) Pixels as a set of wide-angle edgels; (**b**) a final rete ridge contour after spur-edge removal followed by chain coding. Since the contour obtained in (a) was imperfect because of unconnected pixels, it was necessary for gaps between pixels to be filled by a sequence of dilation and skeltonization. The operation also produced undesired spur edges, and thus they were pruned.

normal epithelia (Fig. 3a) or in lower grades of epithelial dysplasia (Fig. 3c) compared to higher grades of epithelial dysplasia or CIS. With malignant transformation, each rete ridge of the twin-pairs began to deform itself and obtained its own new shape independently, resulting in different shapes within the twin pairs in CIS and SCC (Figs. 3d-3f). In addition, the similarity levels of twin-pair rete ridges varied from area to area within the same tissue sections.

Fig. 4a shows an example of the twin-pair rete ridge selected from captured RGB images. It was transformed into a saturation component in HSV color space (Fig. 4b), and its contrast was enhanced (Fig. 4c). Its bilevel image was obtained by Otsu's thresholding (Fig. 4d), from which insignificant artifacts were removed, as shown in Fig. 4e. To obtain the boundary of the rete ridge, wide-angle edgels were extracted from the bilevel image of Fig. 4e. An obtained boundary (Fig. 5a) was fed to a sequence of processing of spurious removal and chain coding, and a continuous boundary of the rete ridge was generated, as shown in Fig. 5b. Finally, every rete ridge of the twin-pairs was isolated into a separate unit, as illustrated in Figs. 6a and 6b, which show two different examples. Their contour descriptors were truncated up to a significant value of 2% to generate robust representations of the rete ridge units, as shown in Figs. 6c and 6d, respectively.

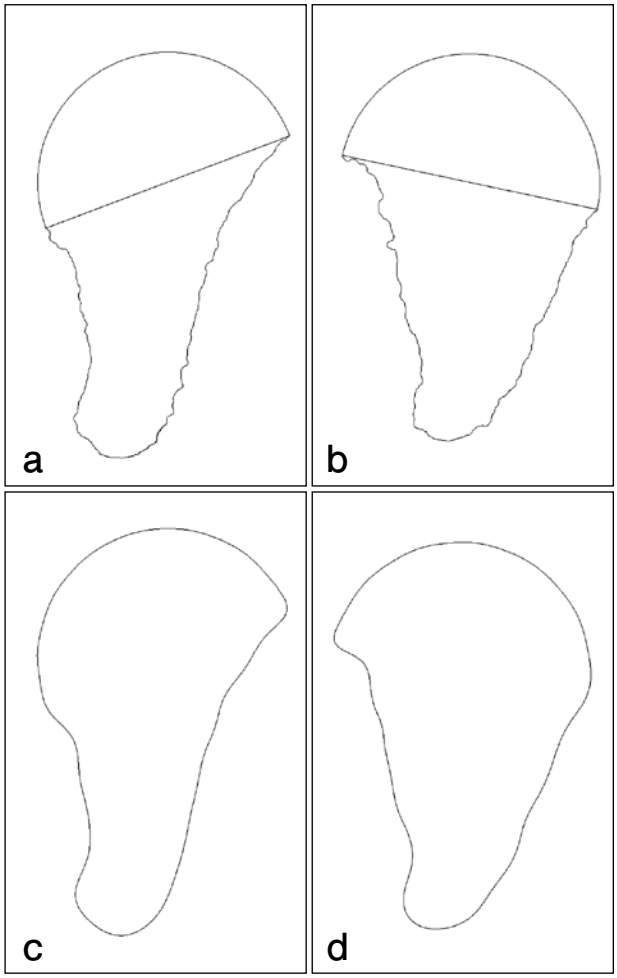

Fig. 6. Isolation of a pair of rete ridge units. (**a, b**) Closed-loop units by placing a half-circle arc onto two end-points of rete ridge twins; (**c, d**) smoothed contours of isolated rete ridge units in (a) and (b), respectively, by assuming a significant 2% value of the contour descriptors.

GUI for twin-pair analysis

For the clinical use of the twin-pair rete ridge analysis, a software package named TwinsViewer was developed (Fig. 7). It included a user-friendly GUI designed to aid pathologists in their clinical testing of the drop-shape similarity between twin rete ridges. Once a targeted twin-pair was identified by a box on a digital microscopic image, all analyses were performed automatically. The output resulted in a pair of the rete ridge units followed by their roundness values and supplementary geometric measurements with respect to their shapes.

Numerical quantification

For reference purposes, the roundness values of different shapes shown in Fig. 8 are listed in Table 1. The roundness value was sufficiently sensitive to drop-shape variations. For example, roundness values were significantly different from each other among objects a, b, and c, which were typical rete ridges seen in higher grades of epithelial dysplasia and CIS. Object e, a half circle, was a rotated version of object d, while the roundness of both of them was identical to 0.5, which is a demonstration of the rotation-invariant property of the roundness defined in this article. The scale-invariance was demonstrated by three objects, g, h, and i, whose roundness values were 0.63 and identical. Object f represents an irregularly shaped unit of the rete ridge obtained from the right rete ridge unit shown in Fig. 6d.

Sample measurement

Table 2 lists the roundness values of left and right twins and their differences for 33 sample images analyzed by the method mentioned above. A higher roundness value among a pair of twins is shown in italics, and the absolute difference with respect to twin-pairs is shown in boldface text in the table. For ease of analysis, Table 2 was converted into Fig. 9, in which the horizontal and vertical axes represent the absolute difference between the left and right rete ridge units of twin-pairs and the representative roundness value of the pair of twins, respectively. It was possible to consider that the drop-shape similarity increases as the roundness difference decreases. Three clusters of plots are clearly separated in the figure. Plots for CIS occupy the top-right area, in which its difference and the roundness levels were higher than those of the other categories. On the other hand, within the interval of low levels of the roundness difference, plots for epithelial dysplasia were distributed throughout the top-left area, and they were represented by their higher roundness and lower difference levels. Plots for normal epithelia are concentrated in the bottom-left area, where their roundness and difference levels were lower than those of any other categories.

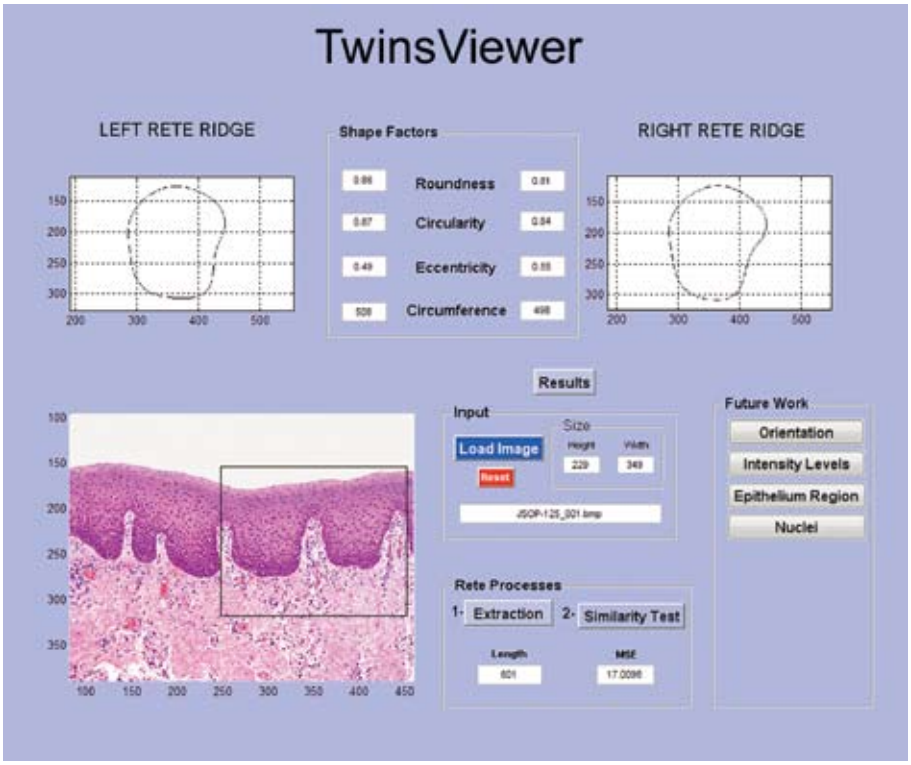

Fig. 7. A graphical user interface (GUI) for the developed method of twin-pair capturing. This GUI was prepared for clinical use of the method. The analysis was performed automatically once twin-pairs of rete ridges were specified.

Discussion

The presence of epithelial dysplasia is generally considered as one of the most important prognostic factors of oral leukoplakia (8, 10). Moreover, the presence of CIS was shown to be significantly associated with recurrence or more advanced progression into invasive SCC (6, 9). However, the histological distinction between CIS and epithelial dysplasia is one of the most challenging issues for pathologists. Since its histopathological evaluation generally depends on an assessment of cellular atypia and arrangements in the epithelial layer, pathologists take into account such various and complicated factors as cellular features, epithelial thickness, cross-cutting, and other histological findings based on their quantitative and qualitative measures which are not evenly weighted but case-dependent proportional weighted. It is thus not surprising that inter- and intra-examiner variabilities in the histopathological diagnosis of oral CIS and grading of oral epithelial dysplasia have often been reported (8, 20-21). The WHO 2005 criteria used for grading epithelial dysplasia included seven architectural and nine cytological criteria (22). One of the most important architectural changes should be alteration of the rete ridges. Rete ridges with a drop-shaped enlargement of their lower part generally result from a monotonous proliferation of basaloid cells, which we have proposed calling a "two-phase appearance" of oral epithelial dysplasia and CIS (6, 9, 11, 23). There should be no arguments on the issue that the rete ridge alteration is the most important issue among the 16 WHO criteria (22). Therefore, we wanted to analyze the rete ridge shape at first by a computer-aided method.

In this study, we have focused our attention on the drop-shaped swelling of rete ridges. Since our concern has been how to distinguish oral borderline malignancies by objective criteria, we have already developed a new

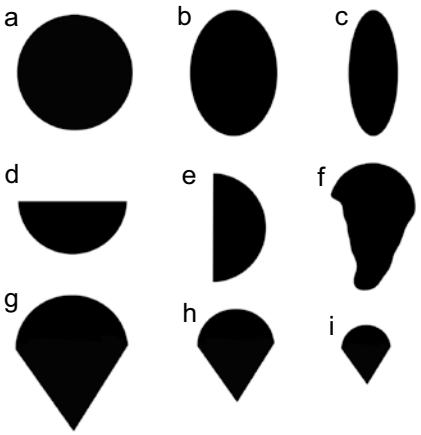

Fig. 8. Examples of objects for a demonstration of scaling-invariance and rotation-invariance. The drop-shape of a rete ridge was quantified by identifying its roundness value. (**a-c**) Different drop shapes; (**d, e**) rotated variants of a half circle; (**f**) an irregular shape of a rete ridge unit as shown in Fig. 6d; (**g-i**) scaled variants of pointed-shapes.

Table 1. Roundness value of different round-shaped objects of Fig. 8.

shape	a	b	c	d	e	f	g	h	i
roundness	1	0.80	0.45	0.50	0.50	0.53	0.63	0.63	0.63

Table 2. Quantitative values of roundness in 33 tissue samples

tissue sample #	histopathological diagnosis	roundness			
		maximum roundness	left	right	difference
1	normal epithelium	0.52	0.45	*0.52*	**0.07**
2	normal epithelium	0.49	0.41	*0.49*	**0.08**
3	normal epithelium	0.39	*0.39*	0.35	**0.04**
4	normal epithelium	0.38	*0.38*	0.32	**0.06**
5	normal epithelium	0.54	*0.54*	0.47	**0.07**
6	normal epithelium	0.25	0.23	*0.25*	**0.02**
7	normal epithelium	0.31	*0.31*	0.28	**0.03**
8	normal epithelium	0.38	*0.38*	0.35	**0.03**
9	normal epithelium	0.37	0.34	*0.37*	**0.03**
10	normal epithelium	0.39	0.32	*0.39*	**0.07**
11	normal epithelium	0.34	0.28	*0.34*	**0.06**
12	epithelial dysplasia	0.61	*0.61*	0.57	**0.04**
13	epithelial dysplasia	0.67	*0.67*	0.64	**0.03**
14	epithelial dysplasia	0.87	0.83	*0.87*	**0.04**
15	epithelial dysplasia	0.75	*0.75*	0.70	**0.05**
16	epithelial dysplasia	0.89	0.82	*0.89*	**0.07**
17	epithelial dysplasia	0.58	0.50	*0.58*	**0.08**
18	epithelial dysplasia	0.75	0.65	*0.75*	**0.10**
19	epithelial dysplasia	0.74	*0.74*	0.66	**0.08**
20	epithelial dysplasia	0.82	*0.82*	0.72	**0.10**
21	epithelial dysplasia	0.80	*0.80*	0.74	**0.06**
22	epithelial dysplasia	0.75	0.68	*0.75*	**0.07**
23	carcinoma in-situ	0.90	*0.90*	0.76	**0.14**
24	carcinoma in-situ	0.72	0.59	*0.72*	**0.13**
25	carcinoma in-situ	0.77	*0.77*	0.63	**0.14**
26	carcinoma in-situ	0.84	*0.84*	0.68	**0.16**
27	carcinoma in-situ	0.70	*0.70*	0.58	**0.12**
28	carcinoma in-situ	0.81	0.62	*0.81*	**0.19**
29	carcinoma in-situ	0.81	*0.81*	0.66	**0.15**
30	carcinoma in-situ	0.88	*0.88*	0.74	**0.14**
31	carcinoma in-situ	0.90	0.80	*0.90*	**0.10**
32	carcinoma in-situ	0.88	*0.88*	0.76	**0.12**
33	carcinoma in-situ	0.91	*0.91*	0.69	**0.22**

diagnostic method by using immunohistochemistry that leads to reasonable distinction of borderline grades (9) based on the current biological concept of cellular differentiation and proliferation (24). However, at the same time, we also intended to develop other objective methods based on different approaches. We believe that our use of a twin-pair method is a sensible approach because the deforming process for each of the twin-pair rete ridges is thought to be independent in terms of direction and speed.

Current cancer biology research notes that some gene mutations in a single cell or in a small number of cells proliferate by communicating with their neighboring cells (25), causing their autonomous and excessive growth, which might result in different degrees of enlargement of the rete ridges from area to area in those lesions.

The rete ridge is an edge segment that can be obtained from the boundary pixels of a segmented epithelial zone (26). Thus, identification of the segmentation was a crucial step, although it did present us with some challenges. These challenges were mainly due to the following: i) staining artifacts, which caused color variations of the biopsy section; ii) lighting acquisition conditions that affected the brightness of different parts of the tissue under the microscope; and iii) the unintentional touching of objects such as lymphocytes. However, we were successful in overcoming these technical difficulties in the present study.

In the past literature, epithelium segmentation has been targeted in some studies, in which different image processing methods were investigated and applied to HE-stained microscopic images (27-28). Landini and Othman isolated the full extent of the epithelial compartment from the underlying connective tissue by optical density thresholding after histogram equalization to obtain a bilevel image of the full epithelial profile (27). The method seems to be simple; however, they did not report on how precise and successful their results were. In addition, their segmentation was not always targeted to the rete ridge representation. In the present study, our main targeted feature was the rete ridge of the epithelium, and it was therefore important to develop a precise segmentation of the epithelium. In the study by Blomgren *et al*., epithelium segmentation was achieved in the green component of the RGB color space (28). Since the contrast between the epithelium and connective tissue was high in the green (G) level values, a thresholding value was clearly determined. In the present study, however, we preferred to obtain the epithelium segmentation by generating the saturation component of the HSV color image, in which the contrast was also high. We intended not to use any color-based segmentation methods because the color variations by staining artifacts could be higher than those of the saturation variation.

In the present study, we could obtain the epithelium segmentation on the basis of our assumption that HSV color space would contain a saturation component which provided a better contrast between the epithelium and connective tissue zones. The epithelial zone had a lower saturation value while the connective tissue zone had a higher saturation value. The contrast between these two main zones was improved by applying the intensity adjustment method. Our application of the global thresholding method to the images was successful in creating bilevel images based on the intensity values of the adjusted saturation images. Since the epithelium and other objects from the connective tissue falling within the same intensity range were segmented together, most parts of the connective tissue were reasonably eliminated. Thus, the epithelial zone was handled as one connected large object, and the other smaller objects were separated into the connective tissue zone. However, some of them were histologically parts of the epithelium, and it was necessary to connect these very close objects to the

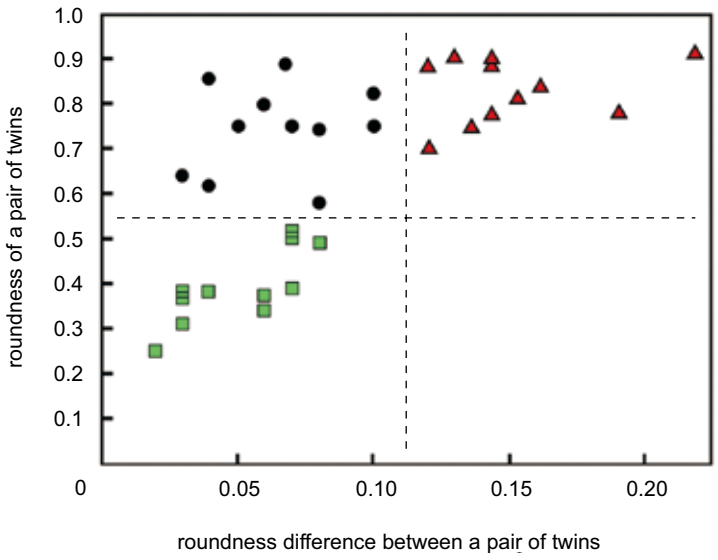

Fig. 9. Plot of roundness values vs. roundness differences in 33 oral epithelial lesions. ■, Normal epithelia; ●, epithelial dysplasia, moderate; ▲, CIS. Differences between roundness values in the *X*-axis and roundness levels in the *Y*-axis. Note that the similarity level increases as the difference value decreases. There were three clusters of plots. Plots for CIS occupied the top-right area, while those for epithelial dysplasia were distributed throughout the top-left area, and those for normal epithelia were concentrated in the bottom-left area. The figure clearly indicated that the roundness and similarity levels of twin-pairs were lowest and highest, respectively, in the normal samples, while those behaviors were opposite in CIS. The figure also indicates that CIS and epithelial dysplasia were distinguishable based on this evaluation method.

epithelium boundary by bridging and thickening morphological operations.

In the same way, we were able to eliminate some of the unintentionally touched objects, which were considered to be parts of the epithelium, by using a highly-textured operation, known as the wide-angle edgel method, to obtain the main structure pixels of the edge of the rete ridges. The gap between edgel pixels was successfully filled by our dilation-and-thinning morphological operation. It was important to generate a closed-loop shape by adding a half circle arc to each rete ridge unit after the determination of the inner peak point of rete ridges and before the quantification of their drop shapes. Since the roundness value of a half circle of any scale and orientation is always fixed and equal to 0.5, we assumed that every rete ridge was to be equally treated. Smoothing the shape roughness of the obtained closed-loop contour was accomplished by reducing the number of contour descriptors in turn to evaluate their roundness more precisely, as reported in different studies including medical applications (18). Shape factors are different measurement tools that can be used for the numerical representation of features. It was important for us to find a quantitative tool which responded to those drop-shape changes found in the histopathological images. Roundness seemed to be the most reasonable shape factor used for quantification because it actually showed good responses to the histological features of rete ridges in oral mucosal lesions.

It is, of course, still too early to say that the present method could be used as a universal one for differentiating any lesional categories of oral borderline malignancies. However, use of the method enabled us to distinguish between epithelial dysplasia and CIS in many of their captured images. The twin-pair method introduced in the present study might not be incongruous to pathologists, because it is based on the existing fundamentals of histopathology for oral cancer research. This method can be applied to any sites of the oral mucosa including the lips, tongue, gingiva, palate, floor of the mouth, and buccal mucosa. However, this method does not seem to be applicable to atrophic types epithelial dysplasia or CIS (6), which have no obvious rete ridges, although they have a rather higher risk of recurrences or invasive changes.

In conclusion, our automated computer-aided method, developed for quantifying rete ridge units in HE-stained microscopic images of the oral mucosal lesions, was shown to function well in discriminating CIS from epithelial dysplasia by evaluating the roughness among rete ridge units using the roundness values of twin-pairs. The concept of a twin-pair could be fed back to routine diagnostic activities of pathologists. In addition, based on the present study, it seems prudent that the development of additional computer-aided morphometrical devices be pursued collaboratively between both pathologists and engineers.

Acknowledgment

This work was supported in part by Grants-in-Aid for Scientific Research from the Japan Society for the Promotion of Science.

References

1. Parkin DM, Bray F, Ferlay J, Pisani P. Global cancer statistics, 2002. *CA Cancer J Clin* 2005; **55**: 74-108.
2. Sawair FA, Al-Mutwakel A, Al-Eryani K *et al*. High relative frequency of oral squamous cell carcinoma in Yemen: qat and tobacco chewing as its aetiological background. *Int J Environ Health Res* 2007; **17**: 185-95.
3. Tilakaratne WM, Klinikowski MF, Saku T, Peters TJ, Warnakulasuriya S. Oral submucous fibrosis: aetiology and pathogenesis. *Oral Oncol* 2006; **42**: 561-8.
4. Kuruvilla J. Utilizing dental colleges for the eradication of oral cancer in India. *Indian J Dent Res* 2008; **19**: 349-53.
5. Gupta PC, Bhonsle RB, Murti PR, Daftary DK, Mehta FS, Pindborg JJ. An epidemiologic assessment of cancer risk in oral precancerous lesions in India with special reference to nodular leukoplakia. *Cancer* 1989; **63**: 2247-52.

6. Working Committee on New Histopathological Criteria for Borderline Malignancies of the Oral Mucosa. The Japanese Society for Oral Pathology. *Guidelines for Histopathological Diagnosis of Borderline Malignancies of the Oral Mucosa*, a preliminary propossal 2005, the Working Committee on New Histopathological Criteria for Borderline Malignancies of the Oral Mucosa, The Japanese Society of Oral Pathology, Yamazaki Publishing, Niigata, 2005.
7. Sami MM, Kikuchi H, Sawair FA, Al-Eryani K, Saku T. Towards a computer-aided system for the histopathological diagnosis of oral borderline malignancies. *Proc AACR Int Conf* 2008; 115.
8. Pindborg JJ, Reibel J, Holmstrup P. Subjectivity in evaluating oral epithelial dysplasia, carcinoma in situ and initial carcinoma. *J Oral Pathol* 1985; **14**: 698-708.
9. Kobayashi T, Maruyama S, Cheng J, *et al*. Histopathological varieties of oral carcinoma in-situ: Diagnosis aided by immunohistochemistry dealing with the second basal cell layer as the proliferating center of oral mucosal epithelia. *Pathol Int* 2010; **60**: 154-64.
10. Pindborg JJ, Reichart PA, Smith CJ, van der Waal I. World Health Organization International Hisological Classification of Tumours. *Histological Typing of Cancer and Precancer of the Oral Mucosa*. Second Edition. Springer-Verlag, Berlin, 1997.
11. Syafriadi M, Cheng J, Jen KY, Ida-Yonemochi H, Suzuki M, Saku T: Two-phase appearance of oral epithelial dysplasia resulting from focal proliferation of parabasal cells and apoptosis of prickle cells. *J Oral Pathol Med* 2005; **34**: 140-9.
12. Sami MM, Saito M, Kikuchi H, Saku T. A computer-aided distinction of borderline grades of oral cancer. *IEEE Int Conf Image Processing ICIP* 2009; 4205-8.
13. Gonzalez RC, Woods RE. *Digital Image Processing*, Third Edition. Prentice Hall, Old Tappan, 2007.
14. Otsu N. A threshold selection method from gray-level histograms. *IEEE Trans Sys Man Cyber* 1979; **SMC-9**: 62-6.
15. Petrou M, Sevilla P. *Image Processing: Dealing with Texture*. John Wiley, New York, 2006; 1-10.
16. Lam L, S.Lee SW, Suen CY. Thinning methodologies: A comprehensive survey. *IEEE Trans Pattern Analysis Machine Intelligence* 1992; **14**: 869-85.
17. Costa LF, Cesar RM. *Shape Analysis and Classification*. CRC Press, Boca Raton, 2001; 412-20.
18. Rangayyan RM. *Biomedical Image Analysis*. CRC Press, Boca Raton, 2005; 530-81.
19. Shen L, Rangayyan MR, Desautels JEL. Application on shape analysis to mammographic classification. *IEEE Trans Medical Imaging* 1994; **13**: 263-74.
20. Abbey LM, Kaugars GE, Gunsolley JC, *et al*. Intraexaminer and interexaminer reliability in the diagnosis of oral epithelial dysplasia. *Oral Surg Oral Med Oral Pathol Oral Radiol Endod* 1995; **80**: 188-191.
21. Kujan O, Khattab A, Oliver RJ, Roberts SA, Thakker N, Sloan P. Why oral histopathology suffers inter-observer variability on grading oral epithelial dysplasia: an attempt to understand the sources of variation. *Oral Oncol* 2007; **43**: 224-31.
22. Barnes L, Eveson J, Reichart P, Sidransky D. World Health Organization Classification of Tumours. *Pathology and Genetics of Head and Neck Tumours*. IARC Press, Lyon, 2005; 163-208.
23. Takeda T, Sugihara K, Hirayama Y, Hirano M, Tanuma JI, Semba I. Immunohistological evaluation of Ki-67, p63, CK19 and p53 expression in oral epithelial dysplasias. *J Oral Pathol Med* 2006; **35**: 369-75.
24. Alberts B, Johnson A, Lewis J, Raff M, Roberts K, Walter P. *Molecular Biology of the Cell*, Fourth Edition. Garland Science, New York, 2002; 864-1009, 1037-1195.
25. Dakubo GD, Jakupciak JP, Birch-Machin MA, Parr RL. Clinical implications and utility of field cancerization. *Cancer Cell Int* 2007; **7**: 2.
26. Sami MM, Kikuchi H, Saku T. Quantitative analysis of the rete processes for the diagnosis of borderline malignancies in microscopic oral cancer images. *Proc 5th International Workshop on Computational Systems Biology WCSB* 2008; **TICSP41**: 149-52.
27. Landini G, Othman IE. Estimation of tissue layer level by sequential morphological reconstruction. *J Microscopy* 2003; **209**: 118-25.
28. Blomgren B, Johannesson U, Bohm-Starke N, Falconer C, Hilliges M. A computerized, unbiased method for epithelial measurement. *Micron* 2004; **35**: 319-29.

Received December 10, 2009 Accepted January 13, 2010